PAPER

Properties of nanoparticles prepared from NdFeB-based compound for magnetic hyperthermia application

To cite this article: E A Périgo *et al* 2012 *Nanotechnology* **23** 175704

Nanotechnology **23** (2012) 175704 (10pp) doi:10.1088/0957-4484/23/17/175704

Properties of nanoparticles prepared from NdFeB-based compound for magnetic hyperthermia application

E A Périgo[1], S C Silva[2], E M B de Sousa[3], A A Freitas[3], R Cohen[4], L C C M Nagamine[4], H Takiishi[2] and F J G Landgraf[1,5]

[1] Center for Process and Product Technology, Institute of Technological Research, São Paulo, SP 05508-901, Brazil
[2] Materials Science and Technology Center, Nuclear and Energy Research Institute, São Paulo, SP 05508-000, Brazil
[3] Nanotechnology Service, Center of Development of Nuclear Technology, Belo Horizonte, MG 31270-970, Brazil
[4] Physics Institute, São Paulo University, São Paulo, SP 05315-970, Brazil
[5] Polytechnic School, São Paulo University, São Paulo, SP 05508-030, Brazil

E-mail: eaperigo@ieee.org

Received 21 December 2011, in final form 17 February 2012
Published 5 April 2012
Online at stacks.iop.org/Nano/23/175704

Abstract
Nanoparticles were prepared from a NdFeB-based alloy using the hydrogen decrepitation process together with high-energy ball milling and tested as heating agent for magnetic hyperthermia. In the milling time range evaluated (up to 10 h), the magnetic moment per mass at $H = 1.59$ MA m^{-1} is superior than 70 A m^2 kg^{-1}; however, the intrinsic coercivity might be inferior than 20 kA m^{-1}. The material presents both ferromagnetic and superparamagnetic particles constituted by a mixture of phases due to the incomplete disproportionation reaction of $Nd_2Fe_{14}BH_x$ during milling. Solutions prepared with deionized water and magnetic particles exposed to an AC magnetic field ($H_{max} \sim 3.7$ kA m^{-1} and $f = 228$ kHz) exhibited 26 K $\leq \Delta T_{max} \leq$ 44 K with a maximum estimated specific absorption rate (SAR) of 225 W kg^{-1}. For the pure magnetic material milled for the longest period of time (10 h), the SAR was estimated as ~2500 W kg^{-1}. *In vitro* tests indicated that the powders have acceptable cytotoxicity over a wide range of concentration (0.1–100 μg ml^{-1}) due to the coating applied during milling.

(Some figures may appear in colour only in the online journal)

1. Introduction

Hyperthermia is a worthwhile application of magnetic materials (MMs) whose aim consists in destroying tumors by increasing the temperature of the system (cancer cell + MM) while causing the minimum prejudice to healthy tissues.

The heating of the MM occurs by its exposure to a magnetic field of amplitude H and frequency f. Under such conditions, a given amount of heat is released because of hysteresis and/or relaxation losses. These mechanisms are functions of several features of the material, such as the electric conductivity, microstructure and particle diameter [1–3]. Hysteresis losses occur in materials whose particles and/or grains have a larger diameter than that of the single domain diameter (SDD) and are related to the energy necessary to cause the displacement of the magnetic domains. On the other hand, relaxation losses are present in particles which possess a smaller diameter than that of the SDD and are classified into two types: Néel and Brownian. The former occurs because of thermal modification in the magnetic moment direction when the anisotropy energy is overcome; the latter is due to the thermal rotation of the particle in a

given medium (usually liquid) that is counterbalanced by the viscosity of the medium, but the magnetic moment is locked onto the crystal anisotropy axis [3, 4]. A quantitative analysis of the loss mechanisms can be found in [5].

Efforts have been made to develop and/or modify MMs capable of presenting a high heating power to be used as an agent for hyperthermia such as magnetic beads containing nanocrystallites embedded in a carbon matrix and ferrite nanoparticles [6–11]. A more complete list of tested materials is reported in [3].

The most used magnetic nanoparticles for hyperthermia investigations are iron oxides, especially magnetite (Fe_3O_4), because its biocompatibility has already been shown [2]. The particles of this material are commonly prepared by chemical routes [12–16]. These routes frequently involve several reagents and strict time, temperature and pH control of the chemical reactions; moreover, heat treatments are also commonly employed. However, the possibility of obtaining nanoparticles by physical methods, even by recycling magnetic compounds, should also be considered for two main reasons: (i) scientific, because it opens new possibilities to obtain new materials with suitable magnetic properties compared to those currently available; and (ii) economical and environmental, since recycling would also give a beneficial impact in reducing the consumption of new raw material.

In this work, the potential use of nanoparticles prepared from a NdFeB-based alloy with suitable properties for magnetic hyperthermia is shown.

2. Experimental details

NdFeB-based sintered magnets (grade N42) were used as the bulk alloy. Firstly, the samples were thermally demagnetized and their coating was removed by grinding. Secondly, small pieces of the magnets (<6 mm) were placed in a steel hydrogenation vessel that was evacuated to mechanical pump pressure. Next, H_2 was introduced up to a pressure of about 2×10^5 Pa (2 bars) and the material was kept under these conditions for 1 h, which resulted in full decrepitation of the alloy. This material was promptly transferred to a high-energy ball milling jar filled with a mixture of cyclohexane (C_6H_{12}) and oleic acid ($C_{18}H_{34}O_2$) and milled at 900 rpm for periods of time (t) up to 10 h. To protect the equipment from failure, the milling was interrupted for one hour after each hour of working time. For $t < 1$ h, the powder was prepared without milling interruption. The milling bodies (spheres) mass to MM mass ratio was 10:1.

Structural characterization of the particles was carried out by high-resolution scanning electron microscopy (HRSEM), transmission electron microscopy (TEM) and x-ray diffraction (Cr-radiation, $30° \leq 2\theta \leq 120°$, scanning rate of $0.5° \text{ min}^{-1}$). In order to evaluate the existence of additional iron phases not detected by XRD in the milled materials, transmission Mössbauer spectroscopy using a ^{57}Co source in a rhodium matrix at room temperature and 4.2 K (liquid He) was utilized. The presence of a coating on the magnetic particles was verified based on the carbon quantification of the samples by combustion testing combined with infrared spectrometry.

The magnetic properties of both bulk magnet (remanence J_r, intrinsic coercivity, and maximum energy product BH_{max}) and powder (H_c, magnetic moment per unit mass σ) samples were obtained by a hysteresigraph and a vibrating sample magnetometer, respectively, at room temperature. Regarding the latter, the measurements were carried out using a maximum applied field of $H = 1.59$ MA m^{-1} ($\mu_0 H = 2$ T). In order to study the superparamagnetic behavior and to find the blocking temperature of the nanoparticles a SQUID magnetometer was used, which typically can perform zero-field and field-cooled (ZFC and FC) measurements, i.e., a σ versus T analysis.

The heating profile of the magnetic particles was measured in a custom-designed magnetic-induction hyperthermia chamber reported elsewhere [17]. A three-loop coil was used at a fixed frequency of 228 kHz in the experiments together with an applied magnetic field of ~3.7 kA m^{-1} (~46 Oe). The temperature was monitored by a thermocouple inserted in a solution prepared with deionized water and magnetic particles, based on a 20:1 mass proportion at $T_{initial} = 297$ K (24 °C), and the data were collected manually. The thermocouple area was much smaller (about 40 times) than that of the sample holder area which contained the evaluated solution and did not influence the measurement. Tests were also performed in pure deionized water without any magnetic material and the temperature increase from this blank sample was subtracted from the results obtained for the solution (water + MM).

Finally, the toxicity of the nanoparticles was evaluated by MTT tests. The cell viability was evaluated by using [3-(4,5-dimethyl-2-thiazolyl-2,5-diphenyl-2H-tetrazolium bromide)]. The cells were cultured in Dulbecco's modified Eagle's medium (DMEM) supplemented with 10% fetal calf serum (FCS) and 1% penicillin/streptomycin and incubated at 310 K (37 °C) under 5% CO_2. Upon reaching 80% confluence, cells were trypsinized and cell viability was assessed by Trypan blue exclusion. Phosphate-buffered saline (PBS) was used as positive control and dimethylsulfoxide as negative control. MRC-5 human fibroblast was plated in 96 well culture plates at 2000 cells per well and cultured in 5% CO_2 at 310 K (37 °C) for 24 h. Then, different concentrations of H3 ($t = 3$ h) and H10 ($t = 10$ h) samples varying from 0.1 to 200 μg ml^{-1} were added to the adhered cells. After this period, the cells were incubated with MTT (0.5 mg ml^{-1}) for 4 h. Then, the supernatant containing MTT was removed and 100 μl of DMSO was placed in each well to solubilize formazan crystals. The absorbance was measured by spectrophotometry in a microplate reader UV–visible at 570 nm. Cell survival percentages were determined by the absorbance at 570 nm of a sample of cells grown in the presence of various concentrations of agent and were expressed as the percentage of the cell viability as compared with the blank control. All toxicity experiments were carried out in quadruplicate.

3. Results and discussion

In order to make the description and discussion of the results easier, this section will be divided according to the type of characterization employed.

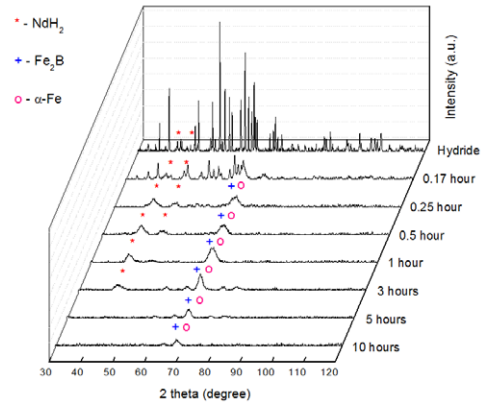

Figure 1. XRD patterns of the powders prepared with different milling times. The single peaks indicated by the cross and circle symbols are related to Fe_2B and/or α-Fe phases.

3.1. (Micro-nano)structural characterization

Figure 1 presents the XRD patterns of all the prepared powders. The hydride ($NdFeBH_x$ − $t = 0$ h) sample shows all the peaks corresponding to the $Nd_2Fe_{14}B$ phase because the original tetragonal crystalline structure does not change after hydrogenation. Furthermore, NdH_2 peaks can also be identified. After milling for 0.17 h (10 min) the intensity of the diffracted peaks is reduced, especially for $2\theta > 90°$, where the original peaks already present a low intensity, which indicates that the crystallite size is reaching a small size (nanometer range). Increasing the milling time by 5 min ($t = 0.25$ h), peaks corresponding to neodymium hydride as well as a broad peak with its center around $2\theta = 70°$ are identified, where the latter corresponds to Fe_2B and/or α-Fe, indicating that the well-known disproportionation reaction has started. This behavior is in agreement with results previously reported by Gang *et al* [18], although in that case the result was obtained after milling for 10 h at 360 rpm under H_2 atmosphere and the soft magnetic phase (α-Fe) was present even in the starting material. For $0.25\ \text{h} \leq t \leq 3$ h, the XRD patterns do not change significantly and, for $t = 5$ and 10 h, the neodymium hydride peaks are no longer observed. This could indicate that this phase became amorphous or, due to the inherent heating during the milling, the hydrogen was removed (at least partially) from the starting material. Indeed, it is believed that the second consideration is plausible because after those milling times (5 and 10 h), the pressure inside the milling jar was higher than atmospheric at room temperature. This has not been observed for shorter milling times.

Figures 2(a)–(d) depict HRSEM images of the powders obtained after milling for $t = 0.17$ h (10 min) and $t = 10$ h. On analyzing the lower magnification images (figures 2(a) and (b)) the particle size difference between the two samples is quite obvious. Besides, the particle shapes and surfaces are also different. The particles prepared with $t = 0.17$ h (10 min) present flat surfaces and sharp edges, suggesting a cleavage fracture, whereas the material milled for $t = 10$ h possesses a rounder shape as well as rough surfaces and agglomerates. On increasing the magnification (figures 2(c) and (d)), it could be confirmed that the particles prepared with $t = 0.17$ h (10 min) also show some roughness on their surfaces, although this feature is not observed for all particles because of the reduced processing time. On the other hand, it seems that each particle obtained after 10 h of milling is an agglomerate constituted of smaller ones of nanometric scale, whose sizes range between 25 and 100 nm (estimated by HRSEM—images not shown). In order to confirm the sizes of these nanoparticles, TEM analysis was carried out. An image of three magnetic nanoparticles and an image of a single nanoparticle in detail are shown in figures 3(a) and (b), respectively. From this last image, it is possible to identify the crystalline planes of the nanoparticle, which indicates that the magnetic phase is not amorphous. Besides, its size ranges within the values previously determined by HRSEM. However, it is not possible to visualize any kind of coating from oleic acid although the carbon concentration in this material is the highest, as listed in table 1.

Table 1. Carbon content of the NdFeB alloy as a function of milling time.

Milling time	% C (wt%)
0 (starting material)	—
0.17 h (10 min)	0.5
1 h	1.4
3 h	3.4
5 h	3.8
10 h	4.4

In order to identify the presence of new iron phases not detected by XRD, the Mössbauer spectra of several samples (starting powder and samples milled for $t = 0.17$, 0.25, 1, 2 and 10 h) were measured at room temperature and are shown in figure 4. The spectrum of the starting powder was analyzed with six sextets of the $Nd_2Fe_{14}BH_x$ phase [19]. The relative areas of the six sub-spectra were fixed to 16:16:8:8:4:4 on the assumption that the recoilless fractions were the same at all the Fe-sites. These sub-spectra were assigned to 4c, 4e, $8j_1$, $8j_2$, $16k_1$, $16k_2$, based on the effective-field order $B_{\text{eff}}(8j_2) > B_{\text{eff}}(16k_2) > B_{\text{eff}}(16k_1) > B_{\text{eff}}(4c) > B_{\text{eff}}(8j_1) > B_{\text{eff}}(4e)$, according to the scheme of Onodera *et al* [19]. After milling, the spectra were analyzed with two more sextets (α-Fe and Fe_2B) and a paramagnetic phase. The parameters of the Mössbauer spectra are shown in table 2. The paramagnetic hyperfine parameters do not correspond to those of the $Nd_{1.1}Fe_4B_4$ phase [20] and are attributed to the Nd-rich intergranular phase [21]. After milling for 0.17 h (10 min), the disproportionation reaction begins to take place, since the Fe population of the $Nd_2Fe_{14}BH_x$ phase decreases to 89.8 % and α-Fe and Fe_2B increase to 6.7% and 0.7%, respectively. On increasing the milling time, the disproportionation reaction continues to take place with reduction of the $Nd_2Fe_{14}BH_x$ phase and increase of the α-Fe and/or Fe_2B phases. Although the NdH_2 phase cannot be detected by ^{57}Fe Mössbauer spectroscopy, its presence is evidenced by x-ray analysis (see figure 1). However, for $t \geq 1$ h, the superparamagnetic relaxation effect begins to be important due to the nanoparticle formation. This effect is clearly seen in figure 4 for

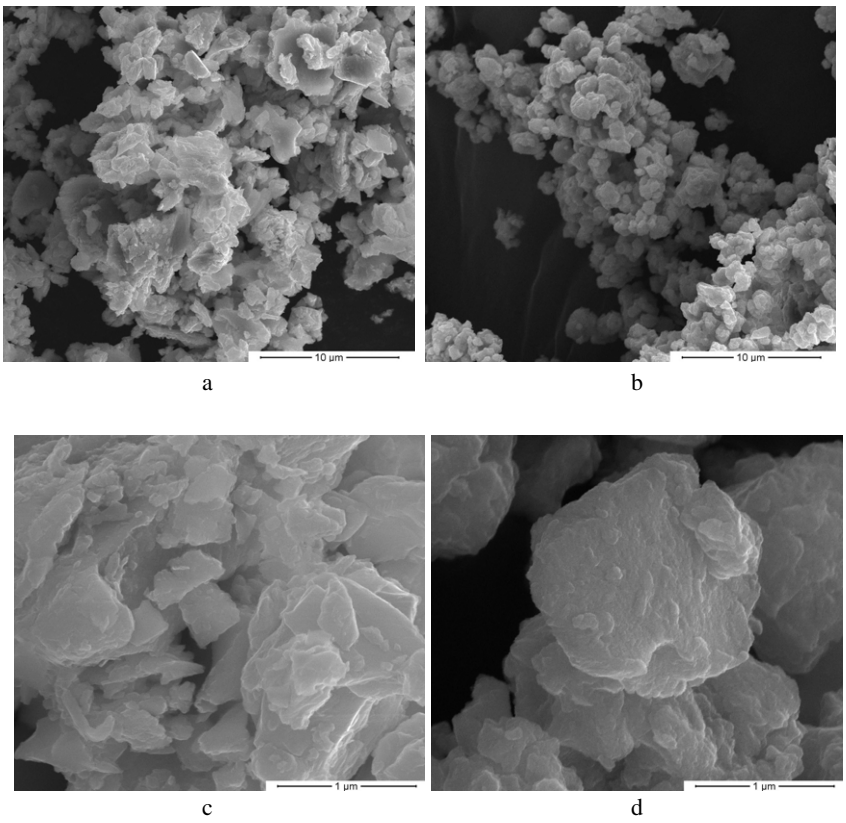

Figure 2. HRSEM images of powders prepared with different milling times: (a) 0.17 h (10 min) and (b) 10 h (both with 10 000× magnification); (c) 0.17 h (10 min) and (d) 10 h (both with 100 000× magnification).

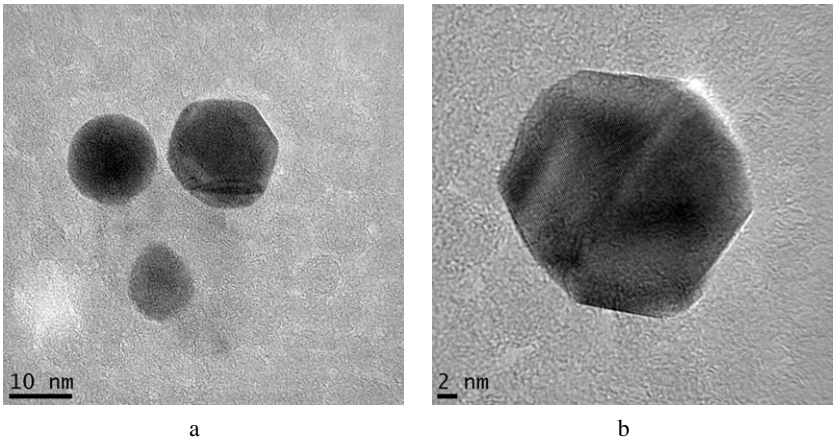

Figure 3. TEM images of particles prepared with $t = 10$ h: (a) general view of three particles and (b) details of a single particle.

$t = 10$ h, for which the Mössbauer spectrum is typical of the iron-based nanoparticles. This spectrum was fitted using one distribution of the hyperfine field, with fixed linewidth (0.3) and H_{eff} varied from 1 to 38 T. In order to avoid magnetic relaxations via thermal excitation and to be able to accompany the disproportionation process, the Mössbauer spectra were measured at 4.2 K for $t = 3$ and 10 h as depicted in figure 5. Although the relaxation effect can also be seen in these spectra, it is clear that, in contrast to the mechanically milled $Nd_{14}Fe_{66.9}Co_{11}B_7Zr_{0.1}Ga_{1.0}$ alloy, where a complete disproportionation reaction was obtained [21], in this work, magnetic nanoparticles of $Nd_2Fe_{14}B$, α-Fe and/or Fe_2B were obtained as a result of an incomplete disproportionation reaction in the intervals of milling time investigated.

3.2. Magnetic characterization

The N42 magnets, before the hydrogen decrepitation process, showed $J_r = 1.28$ T, $H_c = 979$ kA m^{-1} and $BH_{max} = 310$ kJ m^{-3}. Regarding the microstructure, the mean grain size was about 12 μm and no alloying elements were found by EDS (images and spectra not shown).

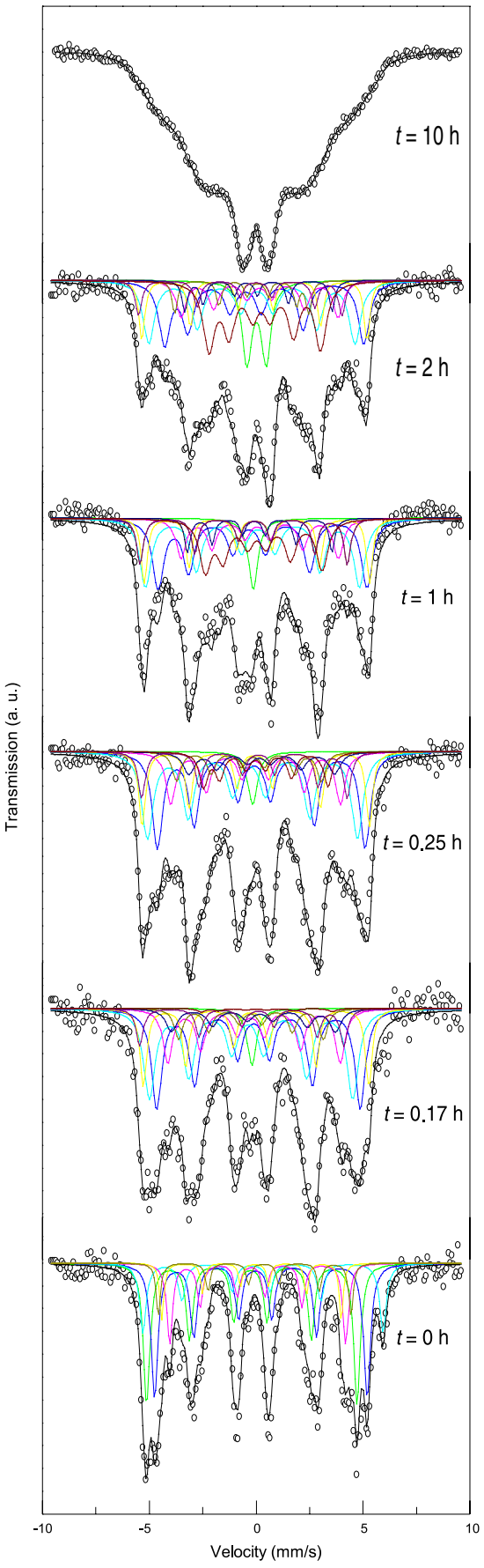

Figure 4. Mössbauer spectra of the prepared powders with different milling times at room temperature.

Table 2. Hyperfine parameters of the original and milled samples for different intervals of time, where IS is the isomer shift, QS is the quadrupole shift, H_{eff} is the hyperfine field and the area is the fraction area of each spectrum.

Time (h)	Phase		IS mm s^{-1}	QS mm s^{-1}	H_{eff} (T)	Area (%)
0	$Nd_2Fe_{14}B$	4c	0.14	−0.42	27.9	100
		4e	−0.15	−0.14	26.0	
		$8j_1$	−0.08	0.31	25.5	
		$8j_2$	0.04	0.54	34.8	
		$16k_1$	−0.24	0.07	30.5	
		$16k_2$	0.09	0.26	30.8	
0.17	$Nd_2Fe_{14}B$	4c	0.02	−0.30	23.7	89.8
		4e	−0.26	0.02	21.0	
		$8j_1$	−0.18	0.158	25.0	
		$8j_2$	−0.13	0.236	32.7	
		$16k_1$	−0.31	0.16	29.5	
		$16k_2$	−0.01	0.23	29.5	
	α-Fe		−0.29	−0.77	29.6	6.7
	Fe_2B		0.26	0.48	19.0	0.7
	paramagnetic		−0.20	0.08		2.8
0.25	$Nd_2Fe_{14}B$	4c	0.20	0.13	21.1	82.4
		4e	−0.24	−0.19	21.0	
		$8j_1$	−0.04	0.02	24.6	
		$8j_2$	−0.04	0.05	32.9	
		$16k_1$	−0.25	0.15	30.4	
		$16k_2$	0.07	0.33	30.1	
	α-Fe		−0.22	−0.66	29.8	8.0
	Fe_2B		0.21	0.47	18.0	6.9
	paramagnetic		−0.17	0.13		2.6
1.00	$Nd_2Fe_{14}B$	4c	0.03	0.27	21.0	73.6
		4e	−0.17	−0.72	20.7	
		$8j_1$	0.11	0.11	22.8	
		$8j_2$	−0.03	0.12	32.7	
		$16k_1$	−0.04	−0.27	31.0	
		$16k_2$	−0.01	0.63	30.3	
	α-Fe		−0.32	−0.52	30.0	8.6
	Fe_2B		0.19	0.33	16.9	15.8
	paramagnetic		−0.14	0.00		2.1
2.00	$Nd_2Fe_{14}B$	4c	−0.19	0.59	21.3	64.8
		4e	−0.30	−0.75	19.4	
		$8j_1$	0.15	0.02	22.7	
		$8j_2$	−0.05	−0.05	32.6	
		$16k_1$	−0.08	0.24	29.9	
		$16k_2$	−0.06	0.87	28.9	
	α-Fe		0.38	−0.74	29.5	6.2
	Fe_2B		0.32	0.16	16.2	20.1
	paramagnetic		0.018	0.90		8.8

Figure 6 depicts the influence of the milling time on the magnetic properties of the prepared NdFeBH-based powders. The magnetic moment per unit mass decreases continuously with the milling time increase, from 131 A m^2 kg^{-1} for the hydride ($t = 0$ h) to 70 A m^2 kg^{-1} ($t = 10$ h), following a monotonic decay. In order to explain this behavior, the discussion of the σ values will be divided into two regions: (i) samples milled up to $t = 1$ h, and (ii) samples milled for $t >$ 1 h. For the former, the most probable cause for σ reduction is the presence of the oleic acid on the particle surfaces after milling. The presence of this coating would decrease the amount of magnetic material per volume and, consequently, σ. To confirm this fact, the particles should present a carbon

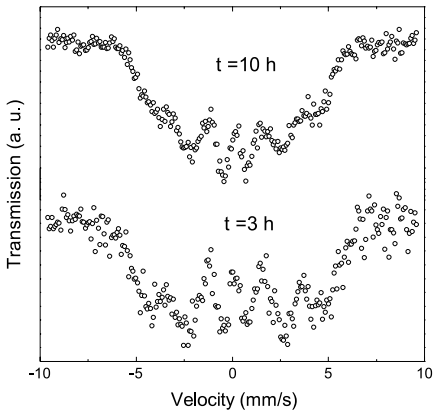

Figure 5. Mössbauer spectra of the powders milled for $t = 3$ and 10 h at $T = 4.2$ K.

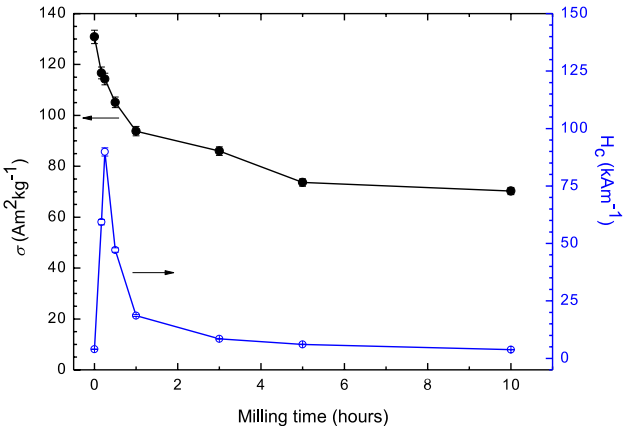

Figure 6. Variation of the magnetic moment per unit mass (σ) and intrinsic coercivity (H_c) at $\mu_0 H = 2$ T of the magnetic powders as a function of the milling time.

content due only to the oleic acid ($C_{18}H_{34}O_2$) because although cyclohexane also has carbon in its composition (C_6H_{12}), it is quite a volatile liquid even at room temperature. This assumption was confirmed after measuring the amount of carbon in powders after several values of t, as listed in table 1. In fact, the amount of carbon on the particles increased continuously with the milling time; however, a second effect also plays a role on σ and must also be taken into account for magnetic powders prepared with larger values of t. It refers to the reduction of the particle size of the $Nd_2Fe_{14}B$-based phase.

On increasing t to periods longer than 1 h, the population of nanoparticles increases and the superparamagnetic relaxation effect, which also reduces the magnetic moment per unit mass as evidenced by the Mössbauer spectroscopy results discussed in the previous section, must also be considered. Therefore, it is expected that the reduction of σ for $t > 1$ h occurs due to the oleic acid coating and relaxation of the magnetic phase, although a quantification of each effect on the magnetic moment per unit mass has not been performed. The obtained values of the magnetic moments, mainly for the samples obtained with $t > 3$ h, might be of the same order of magnitude of those reported for ferrite particles (ranging from 60 to 100 A m^2 kg^{-1} at $\mu_0 H < 1$ T [11, 22–25]).

H_c has a different behavior from that described for σ. The magnetic hydride $Nd_2Fe_{14}BH_x$ prior any milling ($t = 0$ h) has a low intrinsic coercivity because of its low magnetocrystalline anisotropy K (K and H_c are proportional for this class of material [26]). For milling periods of up to 0.25 h, H_c has a linear increase, achieving a value almost one order of magnitude higher than that estimated for the magnetic hydride (prior to milling). This behavior could be explained by considering that the mean particle size, in this milling time range, has become of the same order of magnitude as the magnetic domain of the phase (around 300 nm for the $Nd_2Fe_{14}B$ phase [27]); in this case, the demagnetization of a particle occurs by means of rotation of the magnetic domain, which requires higher fields to be obtained. Another factor which could contribute to the increase of the H_c is the shape anisotropy of the particles, although this effect has not been confirmed in the micrographs reported in the previous sections.

For milling periods longer than 0.25 h, the intrinsic coercivity follows a monotonic decay. This decrease is in agreement with previous reported results regarding the preparation of $Nd_2Fe_{14}B$ nanoparticles [28] and might be ascribed to several reasons: (i) the existence of soft magnetic phases, such as α-Fe and Fe_2B, arising from the disproportionation reaction, which took place during milling and whose intrinsic coercivity should be smaller compared to that of the NdFeB-based phase; (ii) the existence of defects able to create low-energy nucleation sites [28, 29]; (iii) the formation of amorphous structure due to a severe plastic deformation of the particles [29] (especially with the rotational speed used in the present work—900 rpm); and (iv) the presence of superparamagnetic particles, as discussed in the next sections. Although the starting material prior to milling (NdFeB hydride) might be considered a hard magnetic material because its intrinsic coercivity is larger than 1 kA m^{-1} [30], the H_c behavior described in this work is also well known in soft magnetic materials [31, 32]. Figure 7 depicts the hysteresis curves of several powders prepared with different milling times. It is worth noting that the available applied field is not high enough to saturate the magnetization for all samples. However, the slope of the saturation magnetization for $H > 0.7$ MA m^{-1} decreases with t, indicating an increase of the paramagnetic grain size in the range shown [33] or an increase of the particles' anisotropy (see figure 3 of [34]). The hysteresis behavior is due to the blocked particles.

Figure 8 represents the zero-field cooled (ZFC) and field-cooled (FC) curves for some representative samples at low field (~8 kA m^{-1}–100 Oe). A broad maximum on each ZFC curve (indicated by arrows in figure 8) can be seen and results from the large grain size distribution, since each grain size has a distinct blocked temperature. With the increase of t, the temperature for this maximum shifts to higher values. This effect can be related to the increase of the particle size, to the interparticle interactions or to the increment in the dispersion of the anisotropy for a system

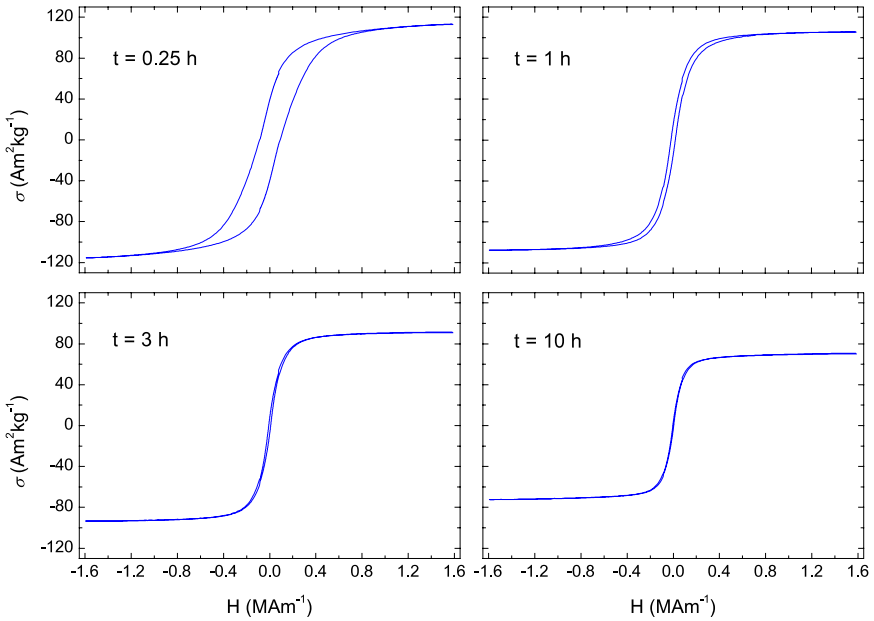

Figure 7. Hysteresis loops for representative samples milled for different times.

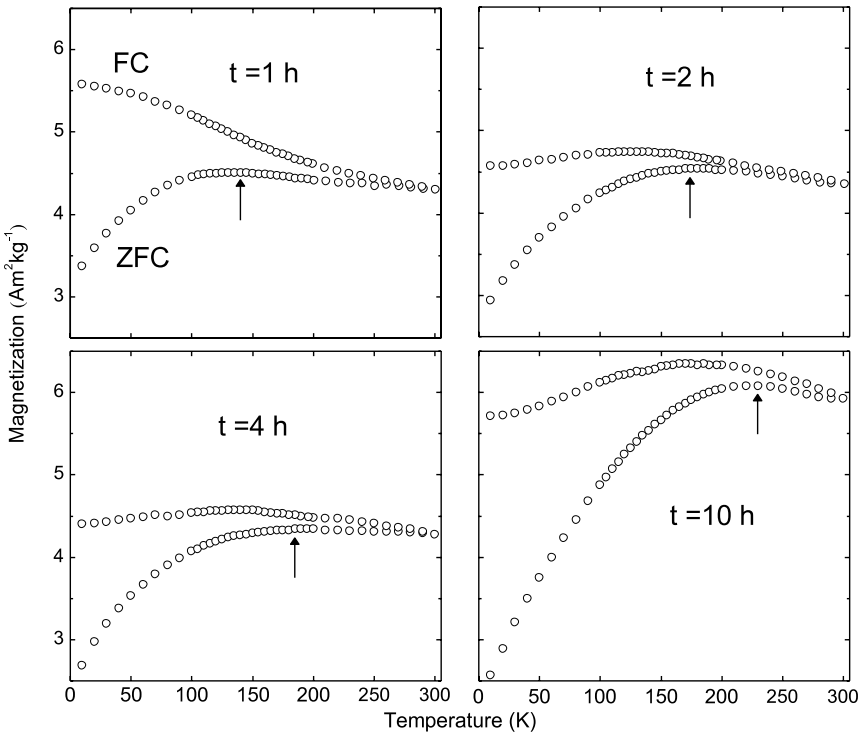

Figure 8. Field-cooled (FC) and zero-field cooled (ZFC) curves measured in $H \sim 8$ kA m^{-1} (100 Oe) for several milling times.

with higher t. However, the Mössbauer results presented in the previous section showed that the relaxation effect increases with t and, as a consequence, the grain size seems to decrease with t. Therefore, it is likely that the increase of interparticle interactions for higher t originates from dipolar interaction and/or the increment in the dispersion of anisotropy can be related to the shift of these temperatures [34, 35]. The presence of the dipolar interactions reduces the population of superparamagnetic particles in favor of blocked ones and this leads to the increase of the average blocking temperature in the low-field regime [34]. The increment in the anisotropy dispersion can be a consequence of the phase variation with t (see table 2) and is also related to the decrease of the slope of the magnetization to attain saturation for higher t (see figure 7 and [34]). An irreversibility temperature (where both FC and ZFC split) occurs for $T > 300$ K for all measured samples (including $t = 1$ and 2 h) and indicates the presence of blocked particles in the range of measured temperature.

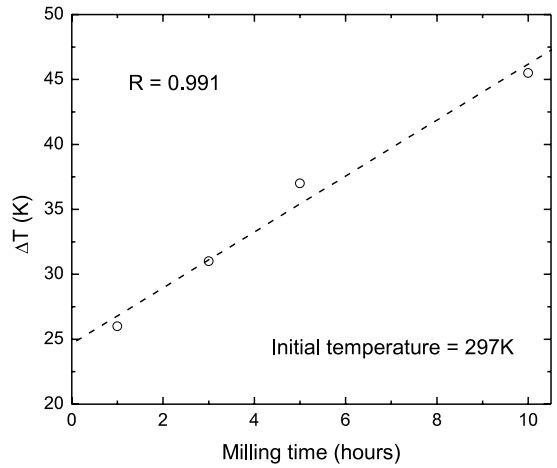

Figure 9. Variation of the temperature increase of the prepared powders as a function of the milling time.

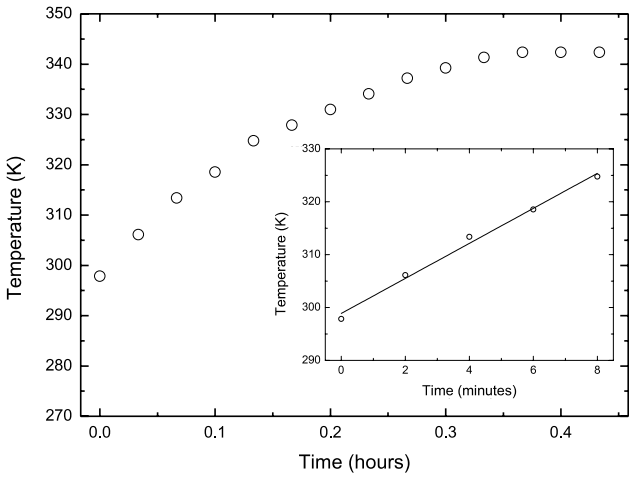

Figure 10. Typical heating profile curve of a magnetic powder prepared in the present work (in this case, $t = 10$ h). The inset depicts in detail the linear portion of the same heating profile.

For $t \geq 2$ h, a decrease in the magnetization is observed in the FC curve when the temperature is decreased from 300 to 4.2 K, indicating the presence of interparticle interactions and corroborating our interpretation given in the sentences above.

3.3. Hyperthermia characterization

Figure 9 depicts the maximum temperature variation (ΔT_{max}) of the magnetic nanoparticles, under $H \sim 3.7$ kA m^{-1} and $f = 228$ kHz, as a function of the milling time. A linear relationship with a high correlation coefficient was obtained. The ΔT_{max} steady state was usually achieved after around 0.5 h, as can be observed in the typical heating profile of the prepared powder depicted in figure 10.

For all evaluated samples, $(T + \Delta T_{max})$ was higher than the recommended hyperthermia treatment temperature, which is reported to be between 313 and 318 K (40–45 °C) [36, 37]. However, these results do not mean that the obtained material cannot be used for such an application, but the experimental conditions employed to evaluate its heating might be reduced, i.e., the applied magnetic field, the frequency, or even both of them. In fact, this must be considered an advantage of this material because it might make possible the use of compact apparatus to provide the needed experimental conditions, which still must be optimized. Although the obtained material is intended to be used in a medical application, it can also be employed for other purposes where localized heating is possible and/or necessary, such as resin curing.

It has also been possible to estimate the specific absorption rate (SAR) of the mixture (deionized water + magnetic particles). The SAR can be expressed by different mathematical expressions. A possible equation is

$$\mathrm{SAR} = \frac{C_p \rho}{m} \left(\frac{\mathrm{d}T}{\mathrm{d}t} \right)_{\mathrm{d}t=0} \tag{1}$$

where C_p is the specific heat, ρ is the magnetic fluid density, m is the magnetic material mass per unit volume of the fluid and $(\frac{\mathrm{d}T}{\mathrm{d}t})_{\mathrm{d}t=0}$ is the rate of temperature increase at the beginning of the heating process [12]. In all SAR experiments, the amount of magnetic material in the solution was the same (proportion 20:1 in mass) and the following expression was employed [38]:

$$\mathrm{SAR} = c \frac{\Delta T}{\Delta t} \tag{2}$$

where c is the specific heat and $\Delta T/\Delta t$ is the initial slope of the heating curve [38]. In order to estimate the SAR correctly, it is necessary to consider the specific heat of the mixture prepared. The $c_{mixture}$ value can be determined by

$$c_{\mathrm{mixture}} = \frac{W_{\mathrm{water}} \times c_{\mathrm{water}} + W_{\mathrm{NdFeB}} \times c_{\mathrm{NdFeB}}}{W_{\mathrm{water}} + W_{\mathrm{NdFeB}}} \tag{3}$$

where W indicates the mass of each constituent of the mixture. As can be verified from equation (3), it has been considered that the magnetic material is fully constituted of the NdFeB-based alloy. Although this is not completely real, as previously verified by XRD and Mössbauer results, the specific heat of NdFeB alloy is of the same order of magnitude as that of iron ($c_{NdFeB} = 560$ J kg^{-1} K^{-1} [39] and $c_{Fe} = 449$ J kg^{-1} K^{-1} [40]). Assuming $c_{water} = 4186$ J kg^{-1} K^{-1}, $c_{mixture} = 4013$ J kg^{-1} K^{-1}. The linear part of the heating curve is shown in the inset of figure 10. The estimated SAR value of the solution prepared with the powder milled for the longest time ($t = 10$ h) is 225 W kg^{-1} and the SAR of this same powdered material (pure) is about 2500 W kg^{-1}. It is worth mentioning that these reported SARs are a function of the chosen H and f values and will possibly change for different conditions. It must be pointed out that although the solid concentration in the solution might be considered high, it is comparable to tests performed in deionized water with superparamagnetic Fe_3O_4 nanoparticles where oleic acid and Tween 80 were used as surfactants [41]; further studies concerning the optimization of the absorption rate of this class of material are in progress. Finally, it is also worth noting that the frequency used in the hyperthermia experiment (228 kHz) is lower than the typical frequency used in Mössbauer spectroscopy (10^8 Hz). As the Mössbauer spectra

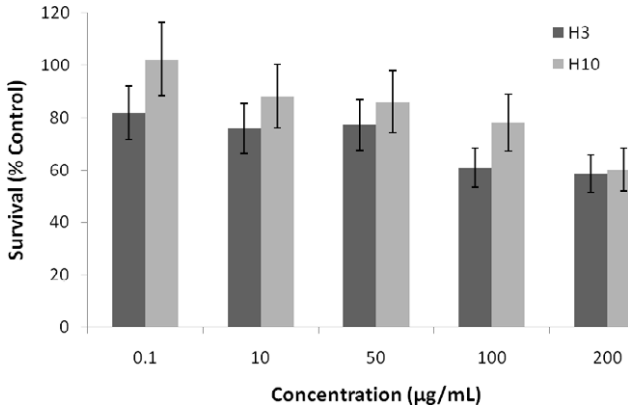

Figure 11. MRC-5 cell viability results from MTT assay after 24 h incubation with H3 ($t = 3$ h) and H10 ($t = 10$ h) samples at 310 K (37 °C), as a function of the particle concentration.

show the presence of the superparamagnetic nanoparticles for $t = 10$ h (see figure 5), this contribution should be higher in the hyperthermia experiment, since the frequency is lower. Therefore, both the blocked (with the hysteresis losses) and the superparamagnetic nanoparticles (Néel and Brownian heating mechanism) are important to the hyperthermia in this system.

3.4. Toxicity characterization

Generally, the cytotoxicity study of materials is essential for further biomedical applications *in vitro* or *in vivo*. Herein, MTT assays were utilized to evaluate the cytotoxicity effect of H3 ($t = 3$ h) and H10 ($t = 10$ h) samples on MRC-5 cell lines. No significant decrease in cell viability was observed for the H10 concentration of 10 μg ml^{-1} at 24 h of incubation as can be seen in figure 11. The decrease in cell viability, in general, appears to be more significant when H3 is used in comparison with H10. The better cell viability for the H10 sample may be attributed to the higher content of carbon, arising from the oleic acid coating, on the surface in this sample when compared with H3 samples. This result indicates that the attachment of carbon on the surfaces of magnetic particles for future bioapplications may provide better morphological structures with increased biocompatible surface areas for improved cell attachment. The cells still maintained more than 50% cell viability after 24 h of treatment for both samples at concentrations as high as 200 μg ml^{-1}. The difference in the cell viabilities of MRC-5 for the two samples is negligibly small for higher concentrations of 200 μg ml^{-1}.

4. Conclusions

The possibility of preparing magnetic particles from the NdFeB-based compound to be used as the heating agent in hyperthermia was presented and discussed. During the $Nd_2Fe_{14}BH_x$ phase milling the occurrence of the disproportionation reaction, confirmed by x-ray diffraction and Mössbauer spectroscopy, was observed, in a similar way to that already observed for the HDDR process performed inside a furnace (closed system). However, this reaction is not complete.

By increasing the milling time, the magnetic moment per unit mass of the powders is reduced because of the coating on the new particles of oleic acid, which also avoids welding of the material to the milling jar, as well as due to the superparamagnetic relaxation effect (assumed for $t > 1$ h). The obtained values are of the same order of magnitude as those of ferrite nanoparticles prepared by chemical routes, which are the most commonly investigated materials for hyperthermia. The intrinsic coercivity presents a similar behavior to that of a soft magnetic material, with a peak of around 95 kA m^{-1} and then presenting a monotonic decay achieving a minimum value of 3.8 kA m^{-1}.

Concerning the structural characterization of the powders, the obtained material after short milling periods of time (0.17 h–10 min) tends to be composed of individual particles. For longer milling times, the particles are agglomerates of nanoparticles whose sizes range from 25 to 100 nm estimated by HRSEM and confirmed by TEM.

Hyperthermia tests have demonstrated that the temperature variation achieved under selected conditions ($H \sim 3.7$ kA m^{-1} and $f = 228$ kHz) increased linearly with milling time. The maximum temperature obtained was around 28 K higher than that recommended for hyperthermia treatment. Therefore the magnetic field amplitude, the frequency, the amount of magnetic material in the solution, or even all of them might be reduced in order to optimize the use of the obtained powders. The estimated SAR of a solution prepared with a material milled for 10 h was 225 W kg^{-1} and for the pure material was about 2500 W kg^{-1}.

Finally, *in vitro* toxicity analyses have demonstrated that the evaluated powders are not prejudicial or the amount used to perform the tests does not cause damage to isolated cells. However, despite the encouraging results, it is not possible to assure the biocompatibility of the particles described in this work because, as explained before, *in vitro* tests are just the first step towards analyzing the investigated material for medical applications.

Acknowledgments

The authors would like to thank IPT, IPEN and CDTN for their facilities. E A Périgo and L C C M Nagamine thank FAPESP (proc. 2010/08018-8 and proc. 2011/50556-0, respectively) for the partial financial support of this investigation. Thanks are also due to M F Moreira, A P Braga, N Ferreira and L Otubo for HRSEM and TEM images.

References

[1] Ichiyanagi Y *et al* 2012 *Thermochim. Acta* **532** 123–6
[2] Hergt R *et al* 1998 *IEEE Trans. Magn.* **34** 3745
[3] Kumar C S S R and Mohammad F 2011 *Adv. Drug Rev.* **63** 789
[4] Fortin J P *et al* 2007 *J. Am. Chem. Soc.* **129** 2628
[5] Rosensweig R E 2002 *J. Magn. Magn. Mater.* **252** 370
[6] Müller R, Dutz S, Habisreuther T and Zeisberger M 2011 *J. Magn. Magn. Mater.* **323** 1223
[7] Ban I *et al* 2011 *J. Magn. Magn. Mater.* **323** 2254–8

[8] Epherre R *et al* 2011 *J. Mater. Chem.* **21** 4393
[9] Skumiel A, Izydorzak M, Leonowicz M, Pomogailo A D and Dzhardimalieva G I 2011 *Int. J. Thermophys.* **32** 1973
[10] Izydorzak M *et al* 2012 *Int. J. Thermophys.* doi:10.1007/s10765-011-1110-z
[11] Sharifi I, Shokrollahi H and Amiri S 2012 *J. Magn. Magn. Mater.* **324** 903
[12] Li Z *et al* 2010 *Mater. Sci. Eng.* C **30** 990
[13] Qu J, Liu G, Wang R and Hong R 2010 *Adv. Powder Technol.* **21** 461
[14] Kikuchi T *et al* 2011 *J. Magn. Magn. Mater.* **323** 1216
[15] Zhao D-L *et al* 2010 *J. Alloys Compounds* **502** 392
[16] Hosono T *et al* 2009 *J. Magn. Magn. Mater.* **321** 3019
[17] Souza K C, Mohallem N D S and Sousa E M B 2010 *J. Sol-Gel Sci. Technol.* **53** 425
[18] Gang S, Lianxi H and Erde W 2006 *J. Magn. Magn. Mater.* **301** 319
[19] Onodera H, Fujita A, Yamamoto H, Sagawa M and Hirosawa S 1987 *J. Magn. Magn. Mater.* **68** 6
[20] Khélifati G, Le Breton J M, Aymard L and Teillet J 2000 *J. Magn. Magn. Mater.* **218** 42
[21] Lianxi H, Yuping L and Yuan Y 2009 *J. Nanosci. Nanotechnol.* **9** 4404
[22] Da Li G *et al* 2010 *Mater. Sci. Eng.* C **30** 148
[23] Parekh K, Upadhyay R V, Belova L and Rao K V 2006 *Nanotechnology* **17** 5970
[24] Kim D-H *et al* 2004 *J. Mater. Sci.* **39** 6847
[25] Lu X *et al* 2011 *Mater. Lett.* **65** 674
[26] Weizhong T, Shouzeng Z and Bing H 1991 *J. Magn. Magn. Mater.* **94** 67
[27] Périgo E A *et al* 2012 *J. Appl. Phys.* **111** 07A725
[28] Simeonidis K *et al* 2011 *Intermetallics* **19** 589
[29] Wang Y, Li Y, Rong C and Liu J P 2007 *Nanotechnology* **18** 456701
[30] David J 1998 *Introduction to Magnetism and Magnetic Materials* 2nd edn (London: Chapman and Hall)
[31] Bahrami A, Hosseini H R M, Abachi P and Miraghaei S 2006 *Mater. Lett.* **60** 1068
[32] Taghvaei A H, Ebrahimi A, Ghaffari M and Janghorban K 2011 *J. Magn. Magn. Mater.* **323** 149
[33] Nagamine L C C M, Mevel B, Dieny B, Rodmacq B, Regnard J R, Revenant-Brizard C and Manzini I 1999 *J. Magn. Magn. Mater.* **195** 437
[34] Kachkachi H and Azeggagh M 2005 *Eur. Phys. J.* B **44** 299
[35] Azeggagh M and Kachkachi H 2007 *Phys. Rev.* B **75** 174410
[36] Ban I *et al* 2011 *J. Magn. Magn. Mater.* **323** 2254
[37] Liangruksa M, Ganguly R and Puri I K 2011 *J. Magn. Magn. Mater.* **323** 708
[38] Wu H, Baker I, Liu Y, Wu X and Cheng J 2011 *Intermetallics* **19** 1517–25
[39] Rabinovich Yu M *et al* 1996 *Intermetallics* **4** 641–5
[40] LideD R (ed) 2005 *CRC Handbook of Chemistry and Physics: A Ready Reference Book of Chemical and Physical Data* p 4.127
[41] Wang Y M *et al* 2011 *J. Magn. Magn. Mater.* **323** 2953